WAVE PROPAGATION IN THE PHOTOSPHERE

BRIGITTE SCHMIEDER
Observatoire de Paris, Meudon, France

(Received 20 October, 1975; in revised form 10 February, 1976)

Abstract. Using a 32 minutes sequence of observation, brightness and velocity fluctuations in the wings of the Mg I line at 5172.7 Å and Fe II line at 5197.578 Å are analysed. The analysis of phase shifts and amplitude ratios leads to the following conclusions:

(1) In the frequency range from $(400\,\mathrm{s})^{-1}$ to $(130\,\mathrm{s})^{-1}$, we find the existence of three modes of waves: internal gravity, evanescent and propagating acoustic waves which appear with increasing frequency. A satisfactory agreement for velocity between observations and theory in the range of horizontal wavelengths >5000 km with a theoretically local relaxation time $\beta^{-1}\sim 80\,\mathrm{s}-40\,\mathrm{s}$ is obtained.

The calculation of intensity fluctuations shows that the Mg I line is sensitive to temperature and density fluctuations while the Fe II line is only sensitive to temperature perturbation. For the best fit with the same value of β^{-1} to both lines (i.e., Fe II and Mg I) it is found necessary that the density effect should be taken into account for the Mg I intensity fluctuations. The relaxation time deduced from observed intensity fluctuations seems to decrease with the period of oscillation. This suggests the presence of a dissipation process.

(2) For higher frequencies oscillations, the phase shift and the amplitude ratios are too small to be interpreted by propagating acoustic waves.

Introduction

Since the discovery of 5 min oscillation by Leighton *et al.* (1962), many theories of wave motions which incorporate observations have been developed (in order to understand this phenomenon). The observations have been summarized in various forms, such as power spectra in spatial and temporal frequencies (Edmonds *et al.*, 1965), energy diagram in two dimensions k, ω (ω is the frequency, k the spatial number) (Mein, 1966; Deubner, 1974). In addition, the phase and amplitude of intensity fluctuations or velocities at two different altitudes have been examined (Evans *et al.*, 1963; Mein, 1971; Sivaraman, 1973; Deubner, 1974). Thus many physical properties of the 5 min oscillations are known as functions of height in the atmosphere, i.e. variations of period, amplitude, spatial wavenumber in the height (Evans *et al.*, 1962; Stein and Leibacher, 1974; Beckers, 1975).

However important questions remain unanswered such as the range of frequencies where propagating waves exist and how the energy is transported from the convective layers to the corona? This study is intended to answer these questions and the study is based on the interpretation of phase shifts and amplitude ratios among velocities and intensity fluctuations observed. In interpreting the observations we utilized the hydrodynamic theory developed for an isothermal atmosphere with a fixed rate of radiative dissipation (Noyes and Leighton, 1963; Souffrin, 1966).

The high quality of spectra and the new computing techniques for reducing the

Solar Physics **47** (1976) 435–460.

data (Mein, 1975) allowed us to obtain new results with better accuracy and reliability.

The manner of data reduction is presented first, followed by a summary of hydrodynamical theory which permitted us to interpret the phase shifts and amplitude ratios of fluctuations at two different altitudes. The theoretical computations of line intensity variations in the perturbed model atmosphere are then presented in which we consider variations of different physical parameters, such as temperature and density. In the last section we discuss the effects of different parameters on the results of interpretation.

1. Observations and Analysis

1.1. Selected lines

In a previous paper (Schmieder, 1972) we showed that the best diagnostic tool is the continuum intensity for density variation, and the intensity of a weak line for the temperature perturbations. In addition, the study of strong line wings is shown to be useful, as well as interesting, since (1) the measure of their intensities can be unaffected by the noise if the slit width of the measurement is selected carefully and (2) the formation height of strong line wings is at a rather denser region of the atmosphere so we can select the wavelengths in the line profile according to the altitude of interest.

Therefore and taking into account the available observational material we select the following two lines: 5172 Å of Mg I as the strong line and 5197.578 Å of Fe II for the weak line in this study.

1.2. Observations

Two sets of spectra were taken simultaneously at the disk center ($\sin\theta \simeq 0.028$) on October 13, 1973 with the spectrograph of the Sacramento Peak solar tower during 32 minutes with intervals of 15 s and the exposure time of 1 s. The slit length is 260 arc seconds. On the first set, the range of the wavelength is 5171 Å to 5178 Å, on the second one, it is 5195 to 5198 Å.

1.2.1. *Calibration Curve*

For each line, a calibration curve was obtained corresponding to the exposure time of 1 s. The linear part of the curve gives a high γ (~ 5). The densities of observed lines are not in this linear part so we associate at each point of lines profile a value of γ_V (Table I) (γ_V in volt $= 2\gamma$).

The density fluctuations measured around these points are small so that we replaced the calibration curve by its tangent.

1.2.2. *Reduction of the Data*

The Mg line wing was scanned with a wavelength step $\Delta\lambda = 0.109$ Å at four wavelengths in each side of the line. The two sets of scans obtained at shorter and

longer wavelengths were separated by 0.6 Å. The slit size of the microphotometer was 0.109 Å × 230 km. For the Fe II line we used a wavelength step $\Delta\lambda = 0.036$ Å and a slit size 0.036 Å × 230 km.

The transmission fluctuations were normalized with respect to the rms value per frame for each wavelength, so that the variations of the seeing throughout the sequence are approximately corrected for average size heterogeneities. On each frame t, at each spatial point x of the spectrograph slit, the profile of the lines were computed by appropriate interpolation formulae (P. and N. Mein, 1975) in the wavelength range $\lambda = 5172.7 \pm 0.3$ Å and $\lambda = 5172.7 \pm 0.55$ Å for the Mg I line and $\lambda = 5197.578 \pm 0.064$ Å for the Fe II line.

In Section 3 we shall present the theoretical calculation of fluctuations of intensity and the velocities for given $\Delta\lambda_j$ (designed by the subscript j for the jth point) from the center of the line profile. We search the corresponding j points in the line profiles by a method described by P. and N. Mein (1975) based on the search of two points separated by $2\Delta\lambda_j$; we obtained the observed fluctuations of intensity, i.e., $I_j(x, t)$ and the velocities, i.e., $V_j(x, t)$. (The velocity is determined as the deviation of the wavelength of the middle point of the interval $2\Delta\lambda_j$.)

We selected $8\Delta\lambda_j$ in the Mg I line and $6\Delta\lambda_j$ in the Fe I line. In Table I examples of $\Delta\lambda_j$ are listed: three for the first line and four for the second.

1.3. Statistical Analysis

Let $f(x, t)$ and $f'(x, t)$ be two normalized fluctuations such as $I_j(x, t)$ or $V_j(x, t)$. The apodized cross-correlation function is defined as

$$R_{ff'}(\Delta t) = r(\Delta t) \int_x \int_t f(x, t) f'(x, t + \Delta t)\, dx\, dt$$

with

$$r(\Delta t) = \frac{L}{L - |\Delta t|} \left(1 - \frac{\Delta t^2}{L^2}\right)^2$$

where $L = 1920$ s and $D = 230\,000$ km are the total length and time duration of the records.

The Fourier transform of the cross correlation function is (Evans *et al.*, 1963)

$$F_{ff'}(\nu) = \int_{-\infty}^{+\infty} R_{ff'}(\Delta t) \exp(2\pi i \Delta t)\, dt.$$

For $f(x, t) = f'(x, t) = V_j$, we express $F_{VV}(\nu) = P_V(\nu)$ and call $P_V(\nu)$ the temporal power spectral at frequency ν. For $f(x, t) = f'(x, t) = I_j$, $F_{ff}(\nu)$ is the time power spectrum relative to intensity fluctuations and we note $F_{II}(\nu) = P_I(\nu)$.

For $f(x, t) = V_j$ and $f'(x, t) = I_j$ or V'_j, or V_j, $F_{ff'}(\nu)$ is the cross power spectrum, we can write $F_{ff'}(\nu) = R + iS$ where R and S are real functions.

The relation between the Fourier components of the two fluctuations f and f' will be described as a function of frequency by:

(1) their phase difference

$$\Phi_{ff'}(\nu) = \arctan S/R;$$

(2) their coherence

$$C_{ff'}(\nu) = \left[\frac{R^2+S^2}{F_{ff}\ F_{f'f'}}\right]^{1/2}.$$

Let us give a definition for the coherence: the coherence is equal to one when the same wave train (same frequency) occurs at the same point on the Sun for the two lines. Since the interval definition of the autocorrelation function is finite, the value of the coherence will represent the proportion of the solar points where the wavetrain has the same frequency for the two lines during the 32 min of the observation.

(3) The amplitude ratios are the ratios between the power spectra $F_{ff}/F_{ff'}$.

For *intensity* we define the amplitude ratio between I and V as

$$A_{IV}(\nu) = \frac{P_I(\nu) 4\sigma_j^2}{P_V(\nu)\xi_j^2};$$

σ_j is the rms value of the intensity fluctuation $I_j(x, t)$,

$$\sigma_j(t_{i'}) = \sqrt{\left(\sum_{i=1}^{N} |I_j(x_i, t_{i'})|^2\right)\Big/ N} \qquad \sigma_j = \frac{1}{n}\sum_{i'=1}^{n} \sigma_j(t_{i'}),$$

n number of spectra and N number of points in a frame at the wavelength λ_j.

For *velocity* we define the amplitude ratio as

$$A_{VV}(\nu) = \frac{H}{\Delta z_{jj'}} \log \frac{P_V(\nu)}{P'_V(\nu)} \frac{\xi_j^2}{\xi_j^2},$$

where $\Delta z_{jj'} = Z_F(j) - Z_F(j')$, $Z_F(j)$ and $Z_F(j')$ are the heights of formation at points

TABLE I

Typical properties of observed data

Line (Å)	$\Delta\lambda$ jÅ	j	$z_{I(km)}$	τ_I	$z_{F(km)}$	τ_F	γ_V	σ_j %	$T_{I(s)}$	ξ_j (km/s)
5172.7	0.3	8	−140	0.08	−139	0.08	5.8	4.65	310	0.464
	0.4	6	−112	0.12	−102	0.13	7.6	4.75	322	0.347
	0.55	2	− 95	0.16	− 80	0.2	11	4.15	328	0.367
5197.578	0.02	6	− 95	0.16	−170	0.05	6.7	3	300	0.37
	0.034	5	− 50	0.3	−130	0.085	8	2.5	308	0.36
	0.054	3			− 54	0.3				
	0.064	2	50	3	0	1	14	3.4	328	0.35

j and j' in the line profile (see 3.3.2), H is the scale height (see 2.1), ξ_j is the mean rms value $\xi_j(t_{i'})$ of the velocity, i.e.,

$$\xi_j(t_{i'}) = \sqrt{\frac{\sum_{i=1}^{N} |V_j(x_i, t_{i'})|^2}{N}} \quad \text{with} \quad \xi_j = \frac{1}{n} \sum_{i'=1}^{n} \xi_j(t_{i'}).$$

In Table I, the values of ξ_j and σ_j are given for different points in the two line profiles; the heights of formation Z_I or Z_F of these points determined by two methods (see 3.3.2) and their corresponding optical depths (τ_I and τ_F) are listed.

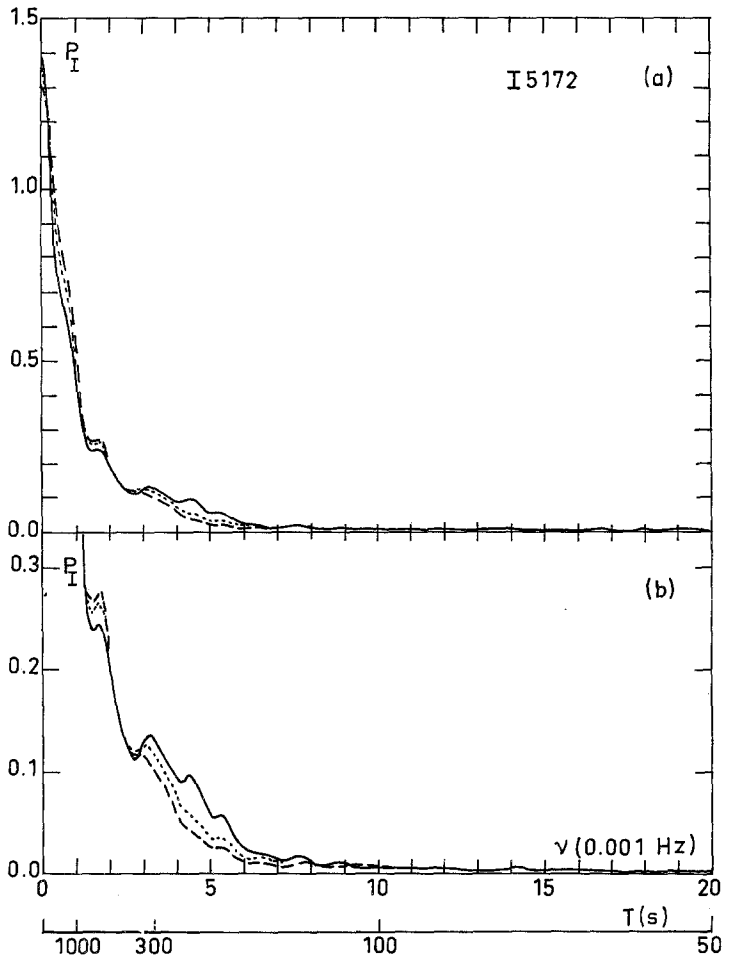

Fig. 1. Time power spectra P of intensity fluctuations at three points in the Mg I line profile; ν is the frequency ($\nu = \omega/2\pi$)

——— $I(8)$ $\Delta\lambda = 0.15$ Å
····· $I(6)$ $\Delta\lambda = 0.3$ Å
------ $I(2)$ $\Delta\lambda = 0.4$ Å

The ordinate scale in (b) is multiplied by a factor 3 to that in (a) to show the details.

1.4. Power spectra

Figures 1 and 2 show, respectively the power spectra P_I for the Mg I line (5172.7) and the iron line (5187.6) and Figure 3 the power spectra P_V for these lines. These are in good agreement with the results of Evans *et al.* (1963). In Table I, the period T_I deduced from the peak of the power spectra (P_I) near 300 s are listed. Apart from the propagation of waves which we consider later, let us discuss the physical significance of these power spectra near the resonance frequencies (i.e., $T_I \sim 300$ s) and for high frequencies.

In the resonance frequency range the convective phenomenon remains important

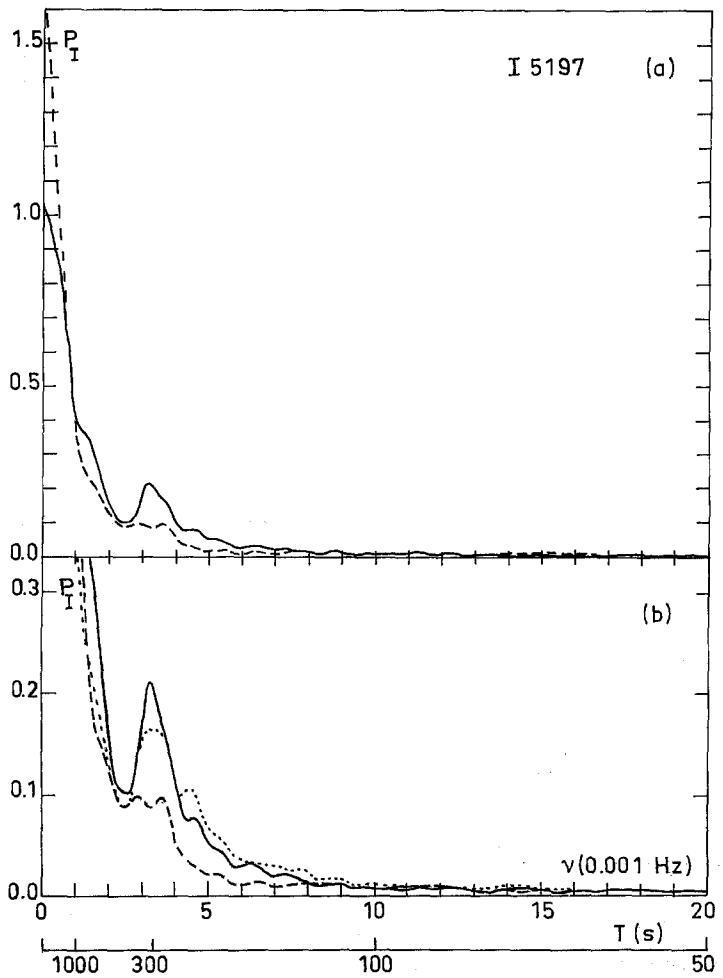

Fig. 2. Time power spectra of intensity fluctuations in 3 points in the Fe II line profile

——— $I(6)$ $\Delta\lambda = 0.02$ Å
····· $I(5)$ $\Delta\lambda = 0.034$ Å
------ $I(2)$ $\Delta\lambda = 0.064$ Å

The ordinate scale in (*b*) is multiplied by a factor equal to 3 compared with the ordinate scale in (*a*).

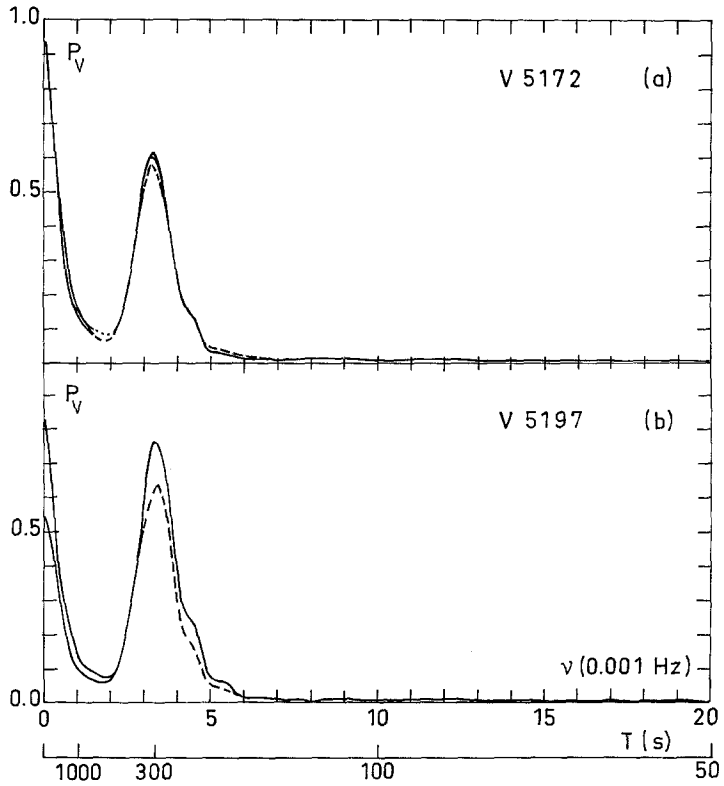

Fig. 3. Time power spectra of velocity fluctuations deduced from Mg I line (*a*) [——— $V(8)$ $V(6)$ ------ $V(2)$] and Fe II line (*b*) [——— $V(6)$ · · · · · · $V(2)$].

and is difficult to separate from the oscillatory phenomenon (Leighton *et al.*, 1962; Mein, 1966; Fossat, 1973, Lynch *et al.*, 1975). After studying spatial filtering, (Mein, 1966) we found little change in the intensity power spectra, so we used another method, a smoothing method based on the search for the limit of $P_I(\nu = 300\,\mathrm{s}, j)$ when the point j corresponds to the deepest level. The ratio between the value $P_I(\nu, j)$ and this limit gives an estimation of the ratio between the oscillatory and convective components at $\nu = 300$ s for different altitudes $Z(j)$. We obtain for the Mg line wings a ratio equal to 0.4 to 1.1 at $Z_I^{(2)} = -95$ km and 2 to 2.5 at $Z_I^{(8)} = -140$ km.

In the high frequency range ($\nu > 4 \times 10^{-3}$ Hz) the energy is greater than 1% of the energy value at $\nu = 0$. We study particularly the 'pollution' of these frequencies by the oscillations of 300 s due to the finite time resolution of our analysis. The energy spectrum of a sinusoid $y = \cos \omega t$ limited in time is a function with a maximum at the frequency ω and secondary lobes located symmetrically with respect to the principal maximum. The existence of a large 300 s peak in the velocity power spectrum suggests the possibility of pollution at frequencies by the presence of secondary maxima, while in the lower frequencies such maxima are insignificant in comparison with convective energy at $\nu = 0$. An estimation of the

energy introduced by this pollution compared to the solar energy at these high frequency gives the ratio $\frac{1}{5}$ between them. This pollution can also introduce a certain phase shift but occurs for frequencies greater than 15×10^{-3} Hz (P. and N. Mein, 1976).

2. Hydrodynamic theory

2.1. Definitions

In the presence of radiative dissipation a small amplitude perturbation δf of quantity f in an isothermal atmosphere in hydrostatic equilibrium can be expressed as

$$\delta f = f_0 \exp\left[\mathbf{kx}+2\pi\nu t\right] e^{i(l+im)z}, \tag{1}$$

where f_0 is the amplitude at certain reference level where the vertical coordinate $z=0$, $\mathbf{k}$ the horizontal wavenumber, $\mathbf{x}$ the horizontal vector, ν the frequency of oscillation and l and m are real numbers. According to Souffrin (1966) the dispersion relation gives

$$(l+im)^2 = a+ib, \tag{2}$$

$$\text{i.e., } a = l^2+m^2, \quad b=\frac{1}{2}\,lm, \tag{3}$$

where

$$a = \omega^2-\omega_a^2+k^2\left[\frac{N^2}{\omega^2}-1\right]-\frac{\beta^2}{\beta^2+\omega^2}\frac{N^2}{\omega^2}\left[k^2-\frac{\omega^4}{g^2}\right] \tag{4}$$

$$b = \frac{\omega}{\beta(\beta^2+\omega^2)}\frac{N^2}{\omega^2}\left[k^2-\frac{\omega^4}{g^2}\right] \tag{5}$$

with

$$\omega_a^2=\frac{\gamma g}{4H}, \quad c^2=\frac{\gamma g}{H}, \quad N^2=\frac{\gamma-1}{\gamma}\frac{g}{H},$$

$$H=\left[\frac{1}{\rho_0}\frac{\mathrm{d}\rho_0}{\mathrm{d}z}\right]^{-1}, \qquad \omega = 2\pi\nu.$$

In the above equations c is the speed of sound, g is gravity, H the scale height, γ the ratio of specific heats, ω_a the cut-off frequency for adiabatic sound waves propagation, N the Brunt Vaisalä frequency, and the subscript zero refers to the initial state. The parameter β represents the effects of dissipation and is given by Spiegel (1957) for an optically thick atmosphere as

$$\beta = \beta'\left(1-\frac{\kappa_c}{k}\operatorname{arc\,cot}\frac{\kappa_c}{k}\right)$$

where $(\beta')^{-1}$ is the relaxation time in an optically thin atmosphere and κ_c is the absorption coefficient for continuum ($\lambda = 5000$ Å) per gram. The values of relaxation time β^{-1} of interest in this study are summarized in Table II.

TABLE II
Relaxation time β^{-1} in s

km \ $L=\frac{2\pi}{k}$	2500	5000	10000
τ_{5000}			
0.05	40	50	80
0.1	20	90	400
0.13	40	100	600

2.2. Limits in the diagnostic diagram

It is known that the curve $g^2k^2=\omega^4$ which is obtained for $b=0$ (Equation 5) separates the diagnostic diagram in the k, ω plane into two parts: one is the domain of propagation of acoustic waves where $\omega^2>gk$ (i.e., $l>0$), and the other is the domain of propagation of gravity waves $\omega^2<gk(l<0)$. This division does not depend on the radiative dissipation.

In the case of adiabatic perturbation we have the following conclusions: (1) for $l=0$, $m\neq 0$ the waves are stationary and evanescent, and (2) for $m=0$, $l\neq 0$ the waves are progressive. In the presence of dissipation, the gradient ml is different from zero regardless of the value of k and ω. The ratio $m/|l|$ characterises the rate of damping per vertical wavelength. The plane (k, ω) is divided in three regions according to the sign of Equation (3) $a>0$ defines two regions of progressive damped waves, and $a<0$ the region of evanescent and 'modified' waves, these regions are separated by two curves of $a=0$. The separation between gravity and acoustic waves ($\omega^4=g^2k^2$) is situated entirely in the region $a<0$.

For given k and β we define two frequencies, $\Omega_a(k, \beta)$ as the cut-off frequency for the existence of progressive acoustic waves ($\omega>\Omega_a$) and $\Omega_g(k, \beta)$ the cut-off frequency for the gravity progressive waves. The values of $\Omega_g(k, \beta)$ are listed in Table III. We give some examples for Ω_a: $k=0$, $\beta^{-1}=80$ s, $\Omega_a=235\ \mathrm{s}^{-1}$ and $k=0$, $\beta^{-1}=0.1$ s, $\Omega_a=220\ \mathrm{s}^{-1}$.

If the wavelength L is larger than 5000 km, it seems difficult to have gravity waves in the range of the 5 min oscillation. For a given k, these two frequencies Ω_a and Ω_g separate the frequency axis in three regions: GW gravity waves, EW evanescent waves, AW acoustic waves.

TABLE III
Values of $\Omega_g(k, \beta)$

$L=\frac{2\pi}{k}$ km \ β^{-1} s	20	40	80
2500	350 s	330 s	280 s
5000	480 s	450 s	400 s

2.3. Phase shift and amplitude ratio between velocity-velocity

The hydrodynamical theory gives us the relations of amplitudes and phase-shifts between different perturbed quantities: V, $\Delta T/T$, $\Delta\rho/\rho$. The velocity ratio at two different levels z_1 and z_2 is defined by

$$\frac{V(z_1)}{V(z_2)} = e^{(z_1-z_2)(1/2H-m)} e^{il(z_1-z_2)}. \tag{6}$$

$\Delta z = z_1 - z_2$, $z_1 = z_F(1)$, $z_2 = z_F(2)$ denotes the altitude of the line formation (Table II). We define the phase shift by

$$\Phi(\Delta z, \beta, \omega, k) = l\Delta z$$

and the amplitude ratio as the logarithm of the velocity ratio, i.e.,

$$A(\beta, \omega, k) = 0.5 - mH,$$

where A is independent of Δz.

For various values of β, $\nu = \omega/2\pi$ and $L = 2\pi/k$, the theoretical curves are computed to be compared with the observational results. Figures 4, 5 and 6 show such comparisons in which ϕ the phase shift, A the amplitude ratio and C the coherence for three pairs of velocities: $V_2(5172)/V_6(5172)$, $V_6(5172)/V_8(5172)$, $V_6(5172)/V_6(5197)$ are plotted. The coherence is good, nearly one, for frequencies lower than 10^{-2} Hz.

On Figure 4 the theoretical curves with $\beta^{-1} = 80$ s and $L > 5000$ km appear to give the best representations of the observations. The disagreement in the range $\nu < 2 \times 10^{-3}$ Hz is due to the granulation which is the predominate phenomenon in this frequency range and the phase shift cannot be interpreted by waves. At $\nu = 2 \times 10^{-3}$ Hz the negative values of the observed phase-shift suggest the existence of downward propagating internal gravity waves.

$\nu = 3.3 \times 10^{-3}$ Hz the agreement is good, the phase-shift values are those of evanescent waves.

$\nu > \Omega_a/2\pi$, the observed phase shift and the amplitude ratio increase according to theory of acoustic waves propagation.

$\nu > 7.5 \times 10^{-3}$ Hz, agreement is lost and we note that observation gives small values of the phase shift and of the amplitude ratio. However the coherence remains good and the velocity power spectra are not zero in this frequency range.

These phases shifts cannot be explained:

(*a*) by acoustic wave theory (the phases increase with the frequency) or

(*b*) by instrumental effects; the guiding errors and distortion due to seeing. Our normalization method of the rms (1,1,2) allows us to test the effects of these errors on the phase ($< 1°$) which seems negligible, or

(*c*) by the 'pollution' phenomenon of the 300 s peak in the high frequencies (1, 4). The 'pollution' effect decreases the phase, and it seems responsible in part for the oscillations of the phase shift curve in the results shown in Figure 4.

Investigations of velocities of other points in Mg I line confirm the existence of

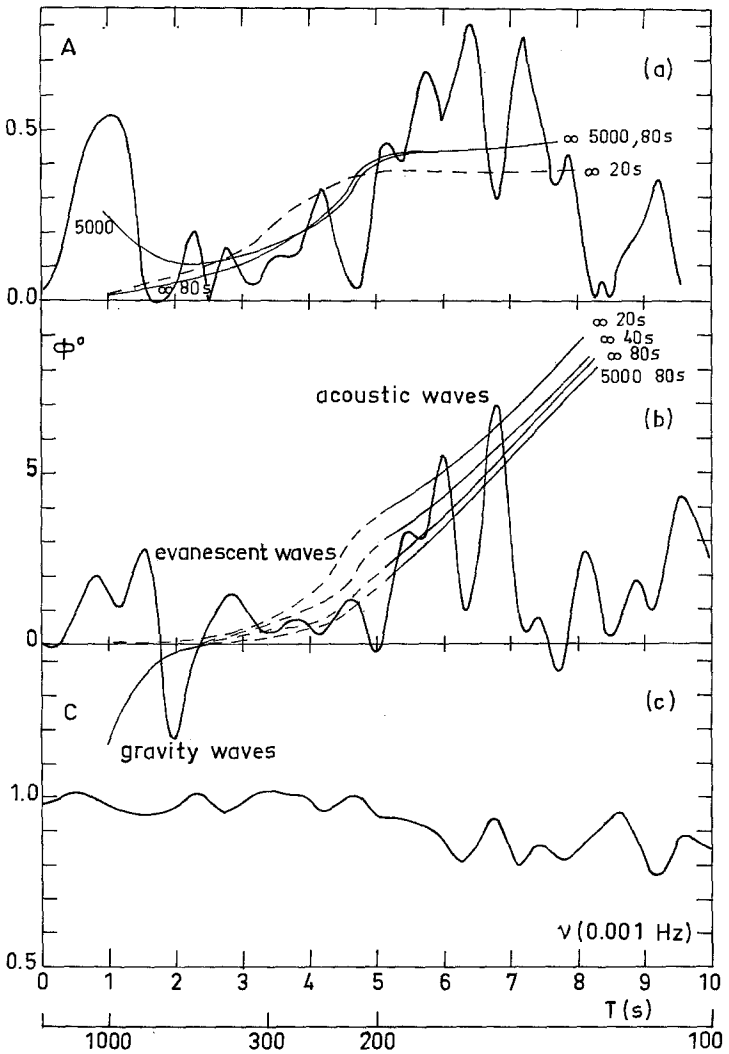

Fig. 4. Amplitude ratio (*a*), phase shift (*b*) and coherence (*c*) of velocities for a pair of points in the Mg I line profile [$V(6)/V(2)$]. The difference in "height of line formation" is $\Delta z = 22$ km; $\tau_{5000} = 0.13$–0.2. Solid lines are observational results, dashed or light curves are theoretical, results with L in km and β^{-1} in s as indicated for each curves.

negative phases at 2×10^{-3} Hz (Figures 5 and 6) related with gravity waves and small phases for high frequencies.

2.4. Phase shift and amplitude ratio of temperature and density relative to velocity fluctuation

The temperature fluctuations can be written for an altitude z

$$\frac{\Delta T}{T}(z) = -\frac{\alpha(\beta)}{c_0} v_m(z) \sin\left[\frac{l'z}{2H} + \Phi\right] \tag{7}$$

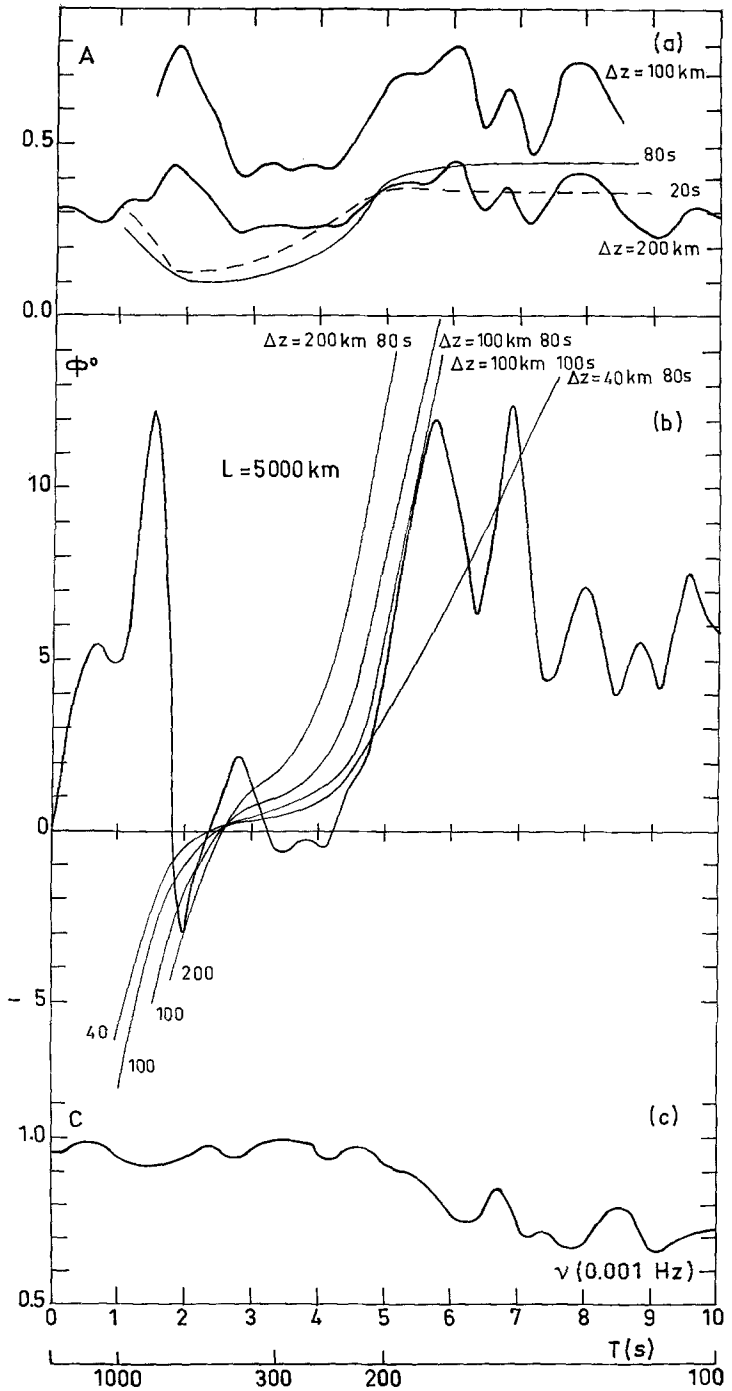

Fig. 5. Amplitude ratio (a), phase shift (b) and coherence (c) for a pair of velocities in the Mg I line $[V(8)/V(6)] - \tau_{5000} = 0.08$–$0.13$. Solid lines are observational results, light or dashed ones are theoretical results obtained with $L = 5000$ km for different values of Δz and β^{-1}.

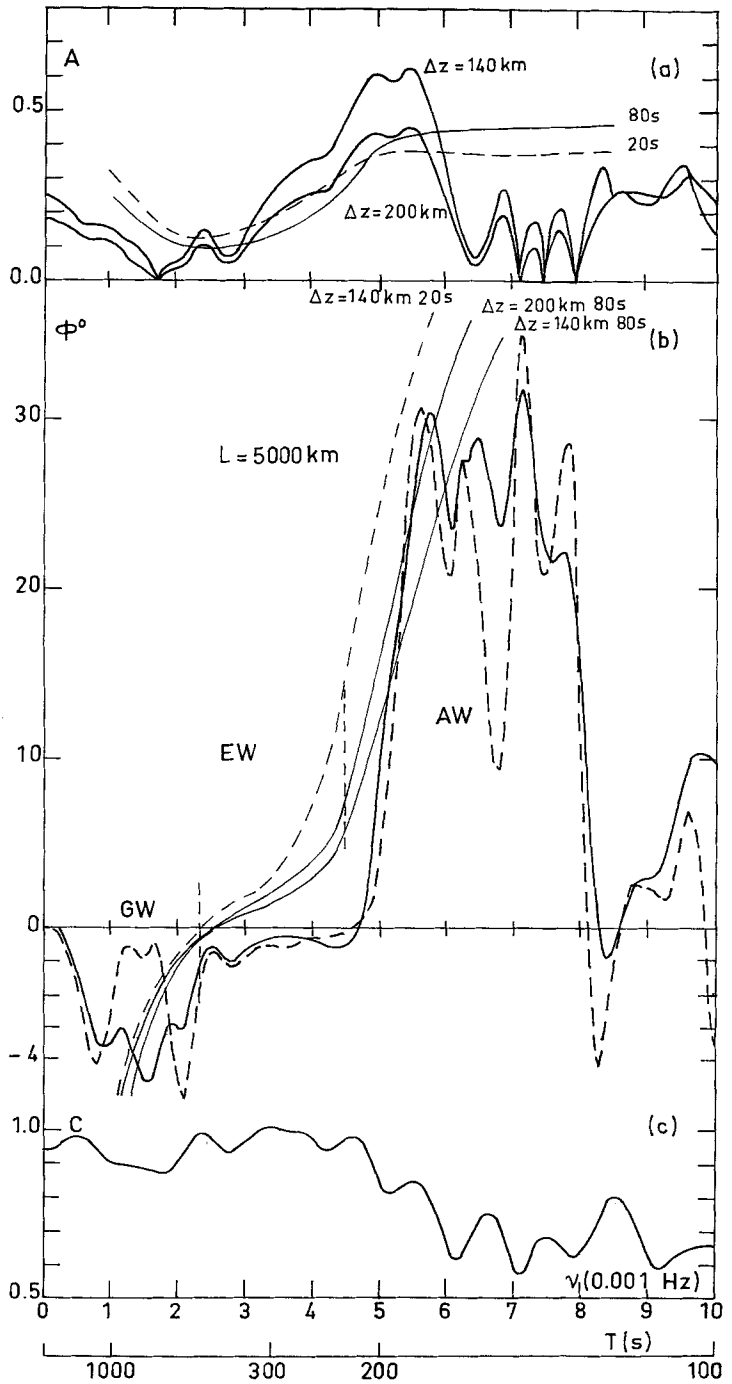

Fig. 6. Amplitude ratio (*a*), phase shift (*b*) and coherence (*c*) for the Mg I line and the Fe II line [5172 $V(6)$/5172 $V(6)$] in (*b*), the heavy solid curves are observational results, the heavy dashed curve represents the phase obtained with a statistical analysis on half of the scanned spectra. The light curves refer to theoretical results with the values of parameter Δ and β^{-1} indicated. Three frequency ranges are indicated as GW for gravity, EW evanescent, and AW for acoustic waves.

and for the density fluctuations, we have

$$\frac{\Delta\rho}{\rho}(z)=\frac{\alpha'(\beta)}{c_0}\,v_m(z)\sin\left(\chi-\frac{l'z}{2H}\right) \tag{8}$$

where c_0 is the isothermal sound speed, $l'=2Hl$, $m'=2Hm$, l and m are defined in Equation (3), v_m is the velocity modulus, $v_m(z)=a_0e^{(l-m')}$ $(z/2H)$ and other quantities are

$$\alpha(\beta)=(\alpha-1)\sqrt{\frac{(l-m')^2+l'^2}{\beta^2+\omega^2}} \tag{9}$$

$$\Phi(\beta)=\pi-\arctan\frac{l'}{l-m'}-\arctan\frac{\omega}{\beta} \tag{10}$$

$$\alpha'(\beta)=\sqrt{\frac{(l-m')^2+l'^2}{\omega^2}} \tag{11}$$

$$\chi(\beta)=\arctan\left[\frac{l-m'}{l'}\right]. \tag{12}$$

Equations (9) and (10) define, respectively, the amplitude ratio and the phase shift between $(\Delta T/T)$ (z) and $v_m(z)$ for $\Delta z=0$, similar relations between $(\Delta\rho/\rho)$ (z) and $v_m(z)$ are given by Equations (11) and (12).

The theoretical results which follow from these equations are shown in Figure 7 for different values of β; for $(\Delta T/T/V)$, $\Phi=90°$ when perturbations are adiabatic $(\beta=0)$ (the curve $\beta^{-1}=80$ s is approximately $\Phi\sim90°$), $\Phi=180°$ when perturbations are isothermal $(\beta\to\infty)$ (the curve $\beta^{-1}=40$ s is approaching this limit). For $(\Delta\rho/\rho/V)$, χ depends weakly on the value of β and χ remains $80°\pm10°$ for adiabatic and isothermal perturbations.

The curves for Φ were given previously by Noyes and Leighton (1963). The calculated quantities $\alpha(\beta)$, $\Phi(\beta)$, $\alpha'(\beta)$, $\chi(\beta)$ refer to pure vertical propagation (i.e., $k=0$) for two reasons: (1) the dependence on k is not very important in the frequency range $\nu>2.5\times10^{-3}$ Hz (see Figure 4 and Section 4) (2) for the frequency lower than 2.5×10^{-3} Hz, the granulation dominates. Thus we limit our study to the frequency range of $2.5-7.5\times10^{-3}$ Hz. Nevertheless, the theoretical results $\alpha(\beta)$, $\Phi(\beta)$, $\alpha'(\beta)$, $\chi(\beta)$ are difficult to compare with the observations because the line intensities are sensitive to simultaneous fluctuations of $\Delta T/T$ and $\Delta\rho/\rho$. This dependence in interpreting the observational results is discussed in the following section.

3. Intensity Fluctuations

3.1. Calculation of line intensity

The calculation of line intensity is performed with the following atmospheric data and atomic data, we adopted the temperature structure given by the

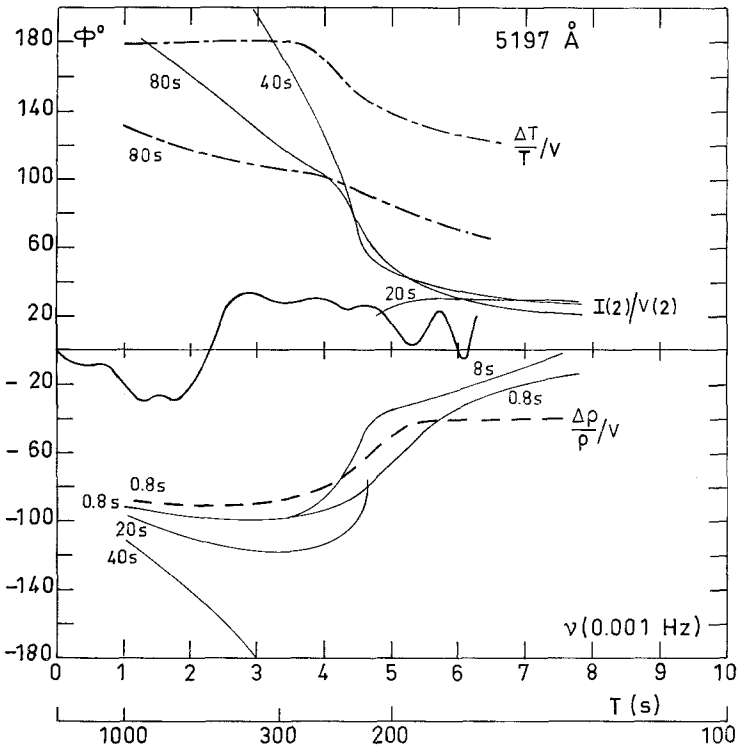

Fig. 7. Phase shift between I/V at the point 2 in the Fe II line. The heavy curves are observational results, the light curves are theoretical results [———$(\Delta I/I)/V$------$(\Delta\rho/\rho)/V$– – –$(\Delta T/T)/V$]. With the value of parameter β^{-1} is indicated.

Gingerich and de Jager (1968) B.C.A., which defined temperature at 70 levels between $10^{-4} < \tau_{5000} < 10$, where τ_{5000} is the optical depth at $\lambda = 5000$ Å. The monochromatic absorption coefficient includes H, H- and He. The microturbulence velocity is chosen constant and equal to 1 km/s (Garz *et al.*, 1969).

The intensities of the Mg I line at 5172 Å and the Fe II line at 5197–578 Å are computed with the following atomic data. Table IV lists the physics parameters used: Xev is excitation potential in electron volt, W equivalent width in mÅ, A abundance of the element, g Gaunt factor, f oscillator strength, CH Van der Vaals constant. For the iron line, we select the product Agf and the constant CH so that W and the central depth agree with the observed values (*Utrecht Atlas* 1960). For the computation of W we take into account the instrumental profile published in the Atlas.

We expressed the temperature and density fluctuations in the model atmosphere as $\Delta T = \alpha T$, $\Delta\rho = \alpha'\rho$. In a previous paper (Schmieder, 1969), we showed that with wave theory the following approximations hold:

$$\frac{\Delta T(z)}{T} = \varepsilon \left(\frac{\rho(z)}{\rho(z_0)}\right)^{-\delta}, \qquad \frac{\Delta\rho(z)}{\rho} = \varepsilon' \left(\frac{\rho(z)}{\rho(z_0)}\right)^{-\delta}.$$

TABLE IV
Atomic Data

Line	Xev	W	log A	log gf	CH	Agf computed	Agf selected
5172.7 Mg I	2.70	1259	7.36[a]	+0.15[e]	3.298×10^{-32}	1.15×10^{-5}	1.15×10^{-5}
			7.48[b]	−0.46[f]			
5197–578 Fe II	3.22	80	6.57[c]	−0.19[g]	3.5×10^{-33}	5.5×10^{-8}	1.2×10^{-7}
			7.6[d]	−0.27[h]		7.5×10^{-7}	

[a] Zwaan (1962).
[b] Lambert and Warner (1968).
[c] Goldberg, Müller, and Allen (1964).
[d] Garz *et al.* (1969).
[e] Corliss and Bozman (1962).
[f] Allen (1962).
[g] Groth (1961).
[h] Warner (1966).

The phase shift between $\Delta T(z)/T$ and $\Delta\rho(z)/\rho$ can be neglected when the vertical wavelength is sufficiently large. The exponent δ was calculated empirically by Mein (1966), and it was 0.07 in the frequency range near $300\,s^{-1}$. The hypothesis of constant relative variation between $\Delta T/T$ and $\Delta\rho/\rho$ is justified by the small value of δ. For given ΔT and $\Delta\rho$, a new electron density at each level is determined by an iterative method using the Saha-Boltzmann equation, then the pressure is obtained from the equation of state. We calculate the intensity of 8 points in the line profile of the Mg I line and of 6 points in that of the iron line for various values of α and α', then the relative variation of intensities $\Delta I/I$ as follows: for a given $\Delta T/T=\alpha$ and $\Delta\rho/\rho=0$, the fluctuation $\Delta I/I$ is equal to αc_T and for $\Delta T/T=0$ and $\Delta\rho/\rho=\alpha'$ we find $\Delta I/I=\alpha' c_\rho$. The results of such independent variations of $\Delta T/T$ and $\Delta\rho/\rho$ are given in Table V at different wavelengths in the lines Mg I 5172 Å and Fe II 5197 Å (Table V). Although shown, we verified that the variation of $\Delta I/I$ are linear with respect to independent fluctuations of $\Delta T/T$ and $\Delta\rho/\rho$. The fluctuations of the temperature $\Delta T/T$ and intensity $\Delta I/I$ are in the same sense, however $\Delta I/I$ decreases when $\Delta\rho/\rho$ increases. If we consider a simultaneous fluctuation of both $\Delta T/T$ and $\Delta\rho/\rho$, the intensity fluctuation can be expressed as

$$\frac{\Delta I}{I}=\left[C_T\frac{\Delta T}{T}-C_\rho\frac{\Delta\rho}{\rho}\right]e^{-i2\pi\nu t}.$$

For example, from Table V we have

$$I_8(5172)=0.07\,\frac{\Delta T}{T}-0.008\,\frac{\Delta\rho}{\rho}$$

$$I_2(5197)=0.0089\,\frac{\Delta T}{T}-0.049\,\frac{\Delta\rho}{\rho}.$$

TABLE V
Computed $\Delta I/I$ for given $\Delta T/T$ and $\Delta\rho/\rho$

λ Å	Designation of wavelength point	$\Delta T/T = 1\%$	$\Delta\rho/\rho = 1\%$
		$C_T = \Delta I/I$ in %	$C_\rho = \Delta I/I$ in %
5172.4	8	7	0.8
5172.3	6	5.6	0.6
5172.15	2	4.2	0.55
5197.578	6	4.4	0.025
5197.558	5	3	0.025
5197.51	2	0.89	0.29

3.2. Phase shift and amplitude ratio between intensity and velocity fluctuations

3.2.1. *Wave Theory*

Using Equations (7) and (8) for $\Delta T/T$ and $\Delta\rho/\rho$ the intensity fluctuations can be expressed as

$$\frac{\Delta I}{I}(z) = [-c_T\alpha(\beta)e^{i\Phi(\beta)} + c_\rho\alpha'(\beta)e^{i\chi(\beta)}]\frac{v_m(z)}{c_0},$$
$$\frac{\Delta I}{I}(z)/v_m(z) = A(\beta)e^{i\phi(\beta)}, \tag{13}$$

where $A(\beta)$ is the amplitude ratio, and $\phi(\beta)$ the phase shift.

Equation (13) shows that for intensity fluctuations caused by T fluctuations, the phase shift $\phi(\beta)$ is equal to $\Phi(\beta)$ and $A(\beta)$ is proportional to $\alpha(\beta)$, if density fluctuations are important, we have two different cases: the perturbations are essentially adiabatic, then the factor relative to $\Delta\rho/\rho$ in Equation (13) leads to a phase shift $\phi(\beta) > \Phi(\beta)$ in the evanescent frequency range and in the acoustic range $\phi(\beta) < \Phi(\beta)$. In contrast, if the perturbations are isothermal $\phi(\beta)$ is negative and $\phi(\beta) = \chi(\rho)$ which is sensitive to the value of β, particularly to small relaxation time.

Amplitude ratios are very sensitive to the relaxation time (see discussion of Figure 12, chapter 4.2.2).

3.2.2. *Observations*

Figures 8 and 9 represent the phase shift $\phi(\nu)$ at two different wavelengths in the Mg I line and three in the Fe II line. The curves in Figure 8 are in good agreement with those obtained for Mg I line by Evans *et al.* (1963). The phase shifts are positive if the positive intensity fluctuations lead upward velocities. In Figure 9c we show the phase shift between I_6(5196 Å) and V_6(5197) also I_6(5197) and V_2(5197) in order to illustrate the difference in the height of line formation at points 2 and 6. This does not introduce any important effect on $\phi(\nu)$.

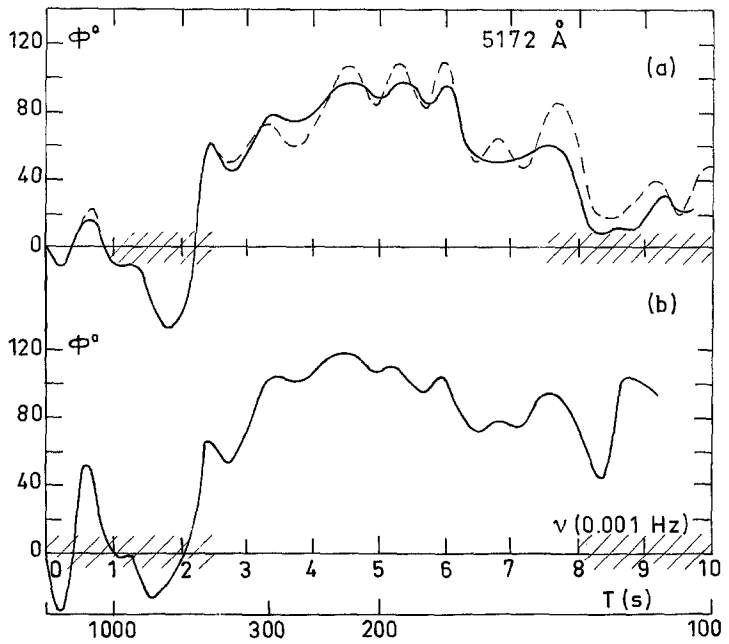

Fig. 8. Phase shift between intensity fluctuations and velocities in the Mg I line deduced observationally (*a*) $I(2)/V(2)$ $\Delta\lambda(2) = 0.55$ Å. The dotted line represents the phase obtained with a statistical analysis on half of the scanned spectra. (*b*) $I(8)/V(8)$ $\Delta\lambda(8) = 0.3$ Å. The hatched regions of the abscissa indicate the frequency range where coherence is <0.4.

3.2.3. *Interpretation of the Phase Shift between the Intensity and Velocity Fluctuations*

The phase shift between intensity and velocity fluctuations gives us three informations (1) in the resonance frequency range, possible discrimination of the effects of granulation (zero phase shift) and traveling waves which produce phase shifts (2) the effects due to variation of the relaxation time and difference in the heights of line formation and (3) the influence of the density fluctuations.

The first and the second effects are examined in terms of the phase shifts at two wavelengths in the Mg I line wing as shown in Figure 10. To achieve the phase shift being caused by the same wave train, we select the coherence > 0.4 for the interpretation of data. This requirement leads us to the frequency range $3 - 8 \times 10^{-3}$ Hz for the following discussions. The theoretical curves shown were computed with the parameters ($C_T = 0.07$, $C_p = 0.008$) and different values of β while we assumed $k = 0$ for purely vertical wave propagation.

(a) *Influence of the granulation.* In Figure 10, we interpret the disagreement between theoretical curves and observations in the frequency range $3 - 4.5 \times 10^{-3}$ Hz as being due to the presence of the granulation which produces zero phase shift. We can calculate that at 300 s the velocity is due 50% to the granulation and 50% to the oscillation phenomenon for $\beta^{-1} = 60$ s at wavelength point 8, i.e. $I(8)/V(8)$,

and that at wavelength point 2(i.e., $I/V(2)$), the contribution from the granulation is $\frac{2}{3}$ and the oscillation $\frac{1}{3}$. The vectorial composition of such phase shift contributions are shown in Figure 11. In the frequency range $>4.5\times10^{-3}$ Hz, the fact that the observational results of $I(2)/V(2)$ lies under $I(8)/V(8)$ can be interpreted as the effects of granulation in the height of line formation of the wavelength point 2 in comparison with the higher height of line formation at wavelength point 8.

(b) *Variation of the relaxation time with the altitude and with the frequency.* The fact of curve of $I(2)/V(2)$ lying under that of $I(8)/V(8)$ in the frequency range $(4.25-7.5\times10^{-3}$ Hz) could be interpreted as in another way. Namely, as seen in Figure 10, the agreement with the theoretical curves with longer relaxation times for the point (2) than point (8) can be interpreted in terms of the difference of the

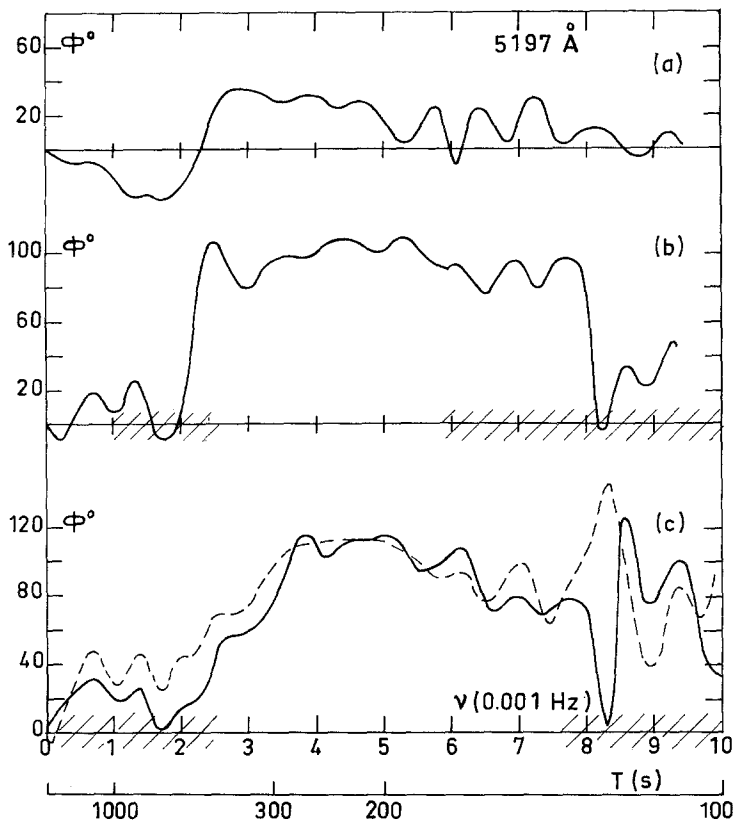

Fig. 9. Phase shift between intensity fluctuations and velocities in the Fe II line as function of ν.

(*a*) $I(2)/V(2)$ $\Delta\lambda = 0.064$
(*b*) $I(5)/V(5)$ $\Delta\lambda = 0.034$
(*c*) $I(6)/V(6)$ $\Delta\lambda = 0.02$

The dotted curve (*c*) represents $I(6)/V(2)$. The hatched range of the abscissa indicates the frequency ranges where the coherence is <0.4.

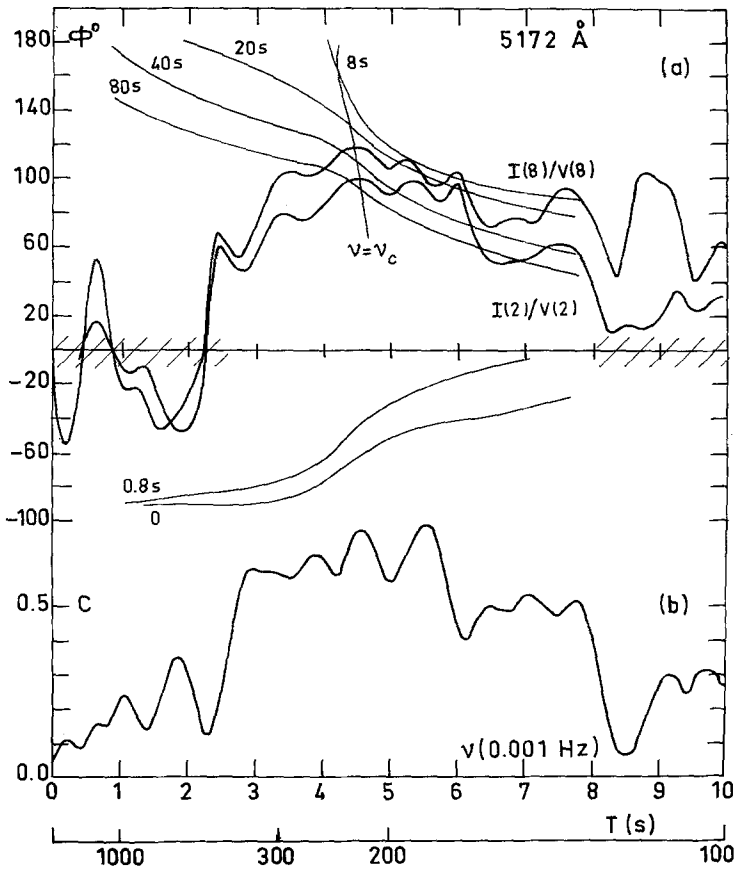

Fig. 10. Phase shift (a) and coherence (b) between intensity fluctuations and velocities in the Mg I line as function of $\nu(I(2)/V(2)-I(8)/V(8))$ (a) the solid curves are observational results, the light curves are theoretical results obtained with $L=\infty$ and β^{-1} as parameter indicated along the curves.

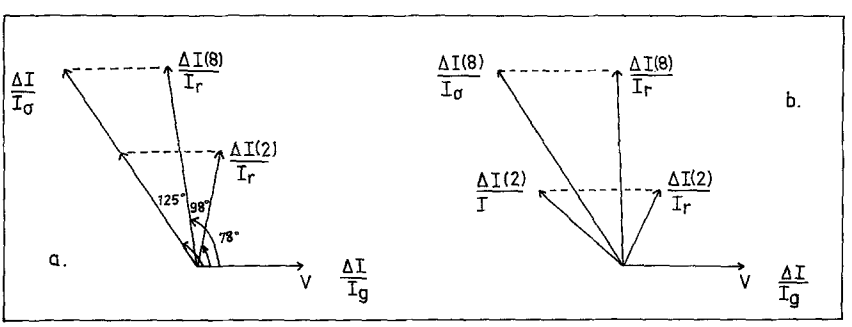

Fig. 11. Vectorial illustration of the superposition of the two effects, i.e. granulation and oscillation at 300 sec^{-1} on $\Delta I/I$ at 2 points in the Mg I line for a given velocity V.

$$a.\ \phi_2\left(\frac{\Delta I}{I}\Big/V\right)_\sigma=\phi_6\left(\frac{\Delta I}{I}\Big/V\right)_\sigma,\quad b.\ \phi_2\left(\frac{\Delta I}{I}\Big/V\right)_\sigma\neq\phi_6\left(\frac{\Delta I}{I}\Big/V\right)_\sigma$$

TABLE VI

Relaxation time β^{-1} at two altitudes at wavelength points 2 and 8 in the wing of Mg I line

$\nu 10^{-3}$ Hz	4.25	6.1	7.5
ν^{-1} s	235	165	135
point 8 ($\tau = 0.08$)	40	20	8
point 2 ($\tau = 0.16$)	80	20	40

relaxation time which decreases with the altitude in an optically thick atmosphere (Mein, 1966). Table VI shows the variation of relaxation time with height in the frequency range of interest.

Table VI suggests that observational results for the point 8 should be interpreted with $\beta^{-1} = 8$ s at 7.5×10^{-3} Hz, $\beta^{-1} = 20$ s at 6×10^{-3} Hz and $\beta^{-1} = 40$ s at 4.25×10^{-3} Hz. A curve connecting these points is clearly a better fit to the data than a constant value of β^{-1} for all frequencies. This variation of the relaxation time with frequency also suggests the dependence of dissipation on wavelength, namely in optically thick atmosphere, waves of shorter horizontal dimension disappear quickly leading to longer β^{-1} for longer wavelength or lines formed higher, i.e., observed $I/V(8)$ curve should agree better with longer β^{-1}. However, Figure 9 is contrary to this statement. Hence, the observed results must be interpreted in terms of contamination by granulation even in the frequency range $4.25 - 8 \times 10^{-3}$ Hz. This point can be seen clearly from Figure 11b in which the resultant phase shifts are shown vectorially. The contribution of the granulation gives a vector $\Delta I/Ig$ at 0°, for the oscillations we have the vectors $\Delta I(8)/I\sigma$ and $\Delta I(2)/I\sigma$, the vectors resultant $\Delta I(8)/Ir$ and $\Delta I(8)/Ir$ show that the effects due to the granulation are more important than those due to the variation of the dissipation characteristic wavelength even at these altitudes $z_I = -100$ or $z_I = -140$ km (Table I).

Deeper in the atmosphere ($z_I = 50$ km) the granulation phenomena predominates and the effects of the oscillations are reduced since the phase shifts are not equal to zero (see Figure 7). For the point (2) in the Fe II line there is no agreement between the theoretical curves, relative to the waves, computed with $C_T = 0.008$ $C_\rho = 0.003$ and the observations.

To examine the influence of the density, we compare the phase shifts between I and V corresponding to two points, one in the Mg I line profile and the other in the Fe II line profile which have the same height of formation and not the same sensitivity to T and ρ fluctuations. The calculations of the height of line formation of the 8 points of the Mg I line and the 6 points in the Fe II line are thus performed as follows.

3.3. Altitudes of the Lines Formation

The notion of height of line formation depends of the physical quantity utilized (Mein, 1966; Mein, 1971; Canfield and Mehltretter, 1973; Beckers, 1975).

Let us suppose that a physical quantity q describing the solar atmosphere, temperature or radial velocity is disturbed by a small quantity $q(z, t)$ which depends on the altitude and time. The corresponding fluctuation of intensity for the wavelength λ can be written:

$$\Delta I_\lambda(t) = \int_{-\infty}^{+\infty} W(z) q(z, t)\, dt.$$

P. Mein (1971) has showed that the function $W(z)$ is a weighting function which depends on z and its maximum defines *an altitude* of formation of ΔI_λ in reference to the physical quantity perturbation.

3.3.1. *Intensity Fluctuations*

We determine an altitude relative to temperature and density fluctuations by a direct procedure (B. Schmieder, 1972). The model atmosphere is disturbed at various levels i with temperature $f(i)$ and density $g(i)$ fluctuations (where i refers to the level number). We look for the levels i_T and i_ρ at which the relative fluctuations of the intensity $\Delta I_\lambda(t)/I_\lambda$ are proportional to $f(i_T)$ and $g(i_\rho)$. These levels are the formation levels of $(\Delta I/I)_\lambda$ with reference to $\Delta T/T$ and $\Delta\rho/\rho$. We find that differences in the values for i_T and i_ρ are small, so we list only one value for these two altitudes z_I in Table I.

The heights of formation of I_2(5172 Å) and I_6(5197.578 Å) happen to be close, thus we use these two lines to consider the influence of density (see Section 4.2).

3.3.2. *Altitude of Velocity Effects*

The formation altitude for the velocities fluctuations z_F (Table I) is defined by the maximum of the contribution function (Elste, 1955), i.e., the depth where the number of atomic elements which form the line is maximum. For the Mg I line, the heights z_F are not very different from the heights z_I. They are in good agreement with those calculated by Altrock and Canfield (1974). For the Fe II line, z_F is higher than z_I.

4. Discussion

4.1. The Dependence of Phase Shift and Amplitude Ratio on Velocity Fluctuations at Different Wavelength Points of a Line Profile

4.1.1. *Dependence on k*

The characteristic length $L = 2\pi/k$ of oscillations is subject to discussions. Mein (1966) and Fossat (1975) have given $L > 10\,000$ km, Deubner (1974) found $L > 6000$ km. We calculate the theoretical curves for two values of L(5000 km, ∞)

but the phase shift and the amplitude ratio are not very sensitive to L as shown in Figure 4.

4.1.2. *Dependence on the Relaxation Time* β^{-1}

For $L = 5000$ km, and at $\tau \simeq 0.08$, (depths where the points 2 and 6 of the Mg I line are formed), Mein (1966) showed that the relaxation time does not vary with small variation of the optical depth (see Table II). In this range of variation of β, the results shown in Figure 4 point out that the variation of β^{-1} does not produce large effects on Mg I line phase shifts.

4.1.3. *Dependence on the Difference of Heights of Line Formation* Δz

Figure 5 shows theoretical curves traced with $L = 5000$ km and for different values of Δz and β^{-1}, i.e.,

$\Delta z^* = 40$ km $\beta^{-1} = 80$ s (this Δz^* is the difference of height of line formulation calculated by contribution functions listed in Table I);

$\Delta z = 100$ km $\beta^{-1} = 80$ s and 100 s,

and

$\Delta z = 200$ km $\beta^{-1} = 80$ s.

It is difficult to obtain a good agreement for the phase and the amplitude ratio with a single set of values β and Δz. In the range of frequencies (2–6.10^{-3} Hz) the agreement is satisfactory with

$$\Delta z < 200 \text{ km and } \beta^{-1} > 80 \text{ s}$$

or with a Δz smaller (150 km) and a relaxation time higher (100 s).

These values of Δz are larger than Δz^* calculated. One explanation can be that the point (8) of Mg line is formed in a non-LTE region. The value founded by Altrock (1974) between these 2 points was also a little larger than our calculated Δz^*.

For the weak iron line we have the same disagreement as seen in Figure 6 ($V_6(5172) - V_8(5197$ Å). The calculated value of Δz^* was 70 km. The agreement appears satisfactory with

$$\Delta z \simeq 200 \text{ km and } \beta^{-1} \simeq 80 \text{ s (Figure 6).}$$

We have done the same investigation for other wavelengths of the iron line. It seems that the Δz^* given by the contribution function methods are too small for the iron line compared with the Mg line.

4.2. THE VARIATION OF PHASE SHIFT AND AMPLITUDE RATIO BETWEEN I/V

The theoretical calculations were made with $k = 0$ (3.2.3.) and the influence of time relaxation values were discussed in 3.2.3.a, now we consider the effects of density fluctuations.

4.2.1. *The Influence of the Density Fluctuations*

The effects of density fluctuations are shown in terms of the phase shifts between $I_2(5172)/V_2$ and $I_6(5197)/V_6$ in Figure 12. The formation heights of these two points are chosen equal, so the effects of granulation are similar for both lines. The Mg line is sensitive to ΔT and $\Delta\rho$ fluctuations while the iron line is only sensitive to ΔT (Table V). In the range of frequencies from 4 to 7.5×10^{-3} Hz, we may select the relaxation time $\beta(\omega)$ by comparing the observational and theoretical results. We see that the relaxation time is of the order of 80 s for $\nu = 4\times10^{-3}$ Hz and decreases to 8 s for $\nu = 7.5\times10^{-3}$ Hz for both lines, in taking into account the fact that Fe II line is sensitive to ΔT and Mg I line is sensitive to ΔT as well as $\Delta\rho$ as mentioned above.

4.2.2. *The Effects of Contrast γ of the Frame*

The amplitude ratios between I and V for the Mg I line shown in Figure 13 are difficult to interpret. We tried to see the influence of the contrast obtained by the calibration curve. We used two values $\gamma_1 = 5.8_v$ and $\gamma_2 = 7_v$ for the point 8 of Mg I line. The theoretical curves are sensitive to the choice of β^{-1}, the observational ones to the value of γ. However the value of γ is more critical than β^{-1} so this may be the main reason of the disagreement between theory and observation. The difficulty of separating oscillation phenomenon and granulation could be mentioned as another cause.

5. Conclusion

The analysis of phases and amplitude ratios for the Mg line and the iron line leads us to a coherent description of the photosphere. In the frequency range from

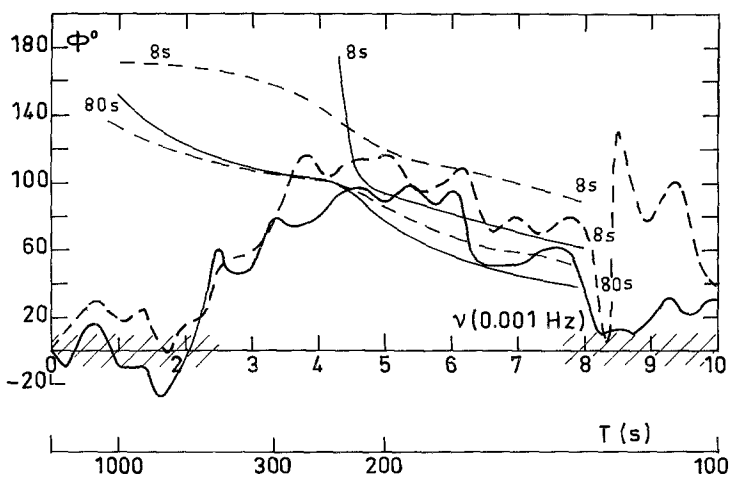

Fig. 12. Influence of the density fluctuation. Phase shifts between I/V for the Fe II line (– – – observation– – –theory) for the Mg I line (———observation———theory).

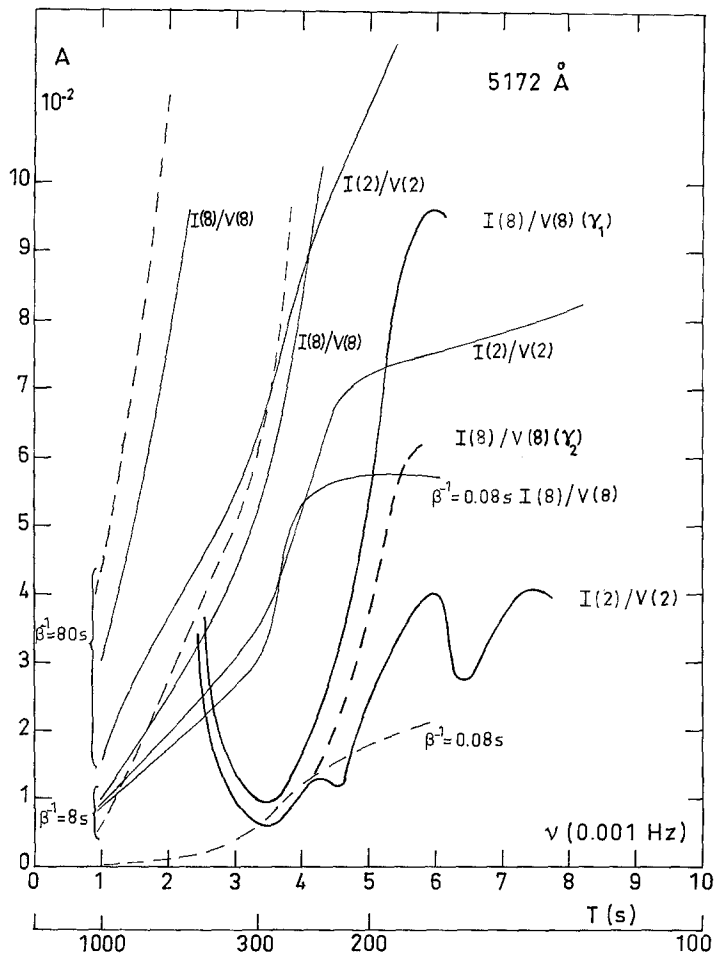

Fig. 13. Amplitude ratio between intensity and velocity fluctuations at 2 points in the Mg I line. The heavy curves are observational results (——$\gamma_1 = 5.8v$, – – –$\gamma_2 = 7v$). The light curves are theoretical results with different values of β^{-1} and $L = \infty$ as well as other parameters (– – –$\Delta T/T/V$, ——$\Delta I/I/V$).

$(400\,\mathrm{s})^{-1}$ to $(130\,\mathrm{s})^{-1}$ we have diagnosed the wave modes: gravity-evanescent and acoustic waves. We obtain a good agreement with values of the horizontal wavelength greater than 5000 km (this is compatible with the two-dimensional analysis, P. Mein, 1966; Deubner, 1974) and for values of the local relaxation time 80 s to 40 s. These values are compatible with the horizontal opacity which results (Spiegel, 1957).

The relaxation time of the temperature fluctuations is a function of the time frequency, is suggests that there is vertical dissipation of great wavenumber ($k_z^{-1} = 1500$ km). This is the first time that density fluctuations have been taken into account for the intensity calculations. It seems that the influence is not negligible for the determination of the relaxation time.

Acknowledgements

The author wishes to thank P. Mein for useful discussions and suggestions, P. and N. Mein for their valuable help in obtaining and reducing the observations. She is also very grateful to J. W. Evans for allowing the use of the Sacramento Peak microphotometer and to Y. Nakagawa for help with this manuscript. The computation was performed on the IBM 360 at the Meudon INAG Center.

References

Allen, C. W.: 1962, *Astrophysical Quantities.*
Altrock, R. C. and Canfield, R. C.: 1974, *Astrophys. J.* **194,** 733.
Beckers, J. M.: 1975, Colloquè No. 250, CNRS.
Canfield, R. C. and Mehltretter, J. M.: 1973, *Solar Phys.* **33,** 33.
Corliss, C. and Bozman, D.: 1962, N.B.S. Monograph No. 53.
Deubner, F. L.: 1974, *Solar Phys.* **39,** 31.
Edmonds, F. N., Michard, R. and Servajean, R.: 1965, *Ann. Astrophys.* **28,** 534.
Elste, G. 1955, Z. Astrophys., 37, 201.
Evans, J. W. and Michard, R.: 1962, *Astrophys. J.* **136,** 492.
Evans, J. W., Michard, R., and Servajean, R.: 1963, *Ann. Astrophys.* **26,** 368.
Fossat, E. and Ricort, G.: 1973, *Solar Phys.* **28,** 311.
Fossat, E.: 1975, Thesis submitted to *Astron. Astrophys.*
Garz, T. *et al.*: 1969, *Astron. Astrophys.* **2,** 446.
Gingerich, O. and De Jager, C.: 1968, *Solar Phys.* **3,** 5.
Goldberg, L. *et al.*: 1964, *Astrophys. J.* **140,** 707.
Groth, H. G.: 1961, *Astrophys. J.* **51,** 231.
Lambert, D. and Warner, B.: 1968, *Monthly Notices Roy. Astron. Soc.* **140,** 195.
Leighton, R. B., Noyes, R. W., and Simon, G. N.: 1962, *Astrophys. J.* **135,** 474.
Lynch, D. K. and Chapman, G.: 1975, *Astrophys. J.* **197,** 241–249.
Mein, P.: 1966, *Ann. Astrophys.* **29,** 153.
Mein, P.: 1971, *Solar Phys.* **20,** 3.
Mein, N. and Mein, P.: 1975, *Solar Phys.* **40,** 317.
Mein, N. and Mein, P.: 1976, *Solar Phys.* in press.
Noyes, R. W. and Leighton, R. B.: 1963, *Astrophys. J.* **138,** 631.
Schmieder, B.: 1969, *C. R. Acad. Sci. Paris,* **269,** 935.
Schmieder, B.: 1972, *Astron. Astrophys.* **16,** 44.
Sivaraman, K. R.: 1973, *Solar Phys.* **33,** 319 and 333.
Souffrin, P.: 1966, *Ann. Astrophys.* **29,** 55.
Spiegel, E. A.: 1957, *Astrophys. J.* **126,** 202.
Stein, R. F. and Leibacher, J.: 1974, *Ann. Rev. Astron. Astrophys.* **12,** 402.
Warner, B.: 1966, *Monthly Notices Roy. Astron. Soc.* **133,** 389.
Zwaan, C.: 1962, *Bull. Astron. Inst. Neth.* **16,** 225.